Urban Air Temperature Model Using GOES-16 LST and a Diurnal Regressive Neural Network Algorithm

Joshua Hrisko [1,*], Prathap Ramamurthy [1], Yunyue Yu [2], Peng Yu [2], and David Melecio-Vasquez [1]

[1] *National Oceanic and Atmospheric Administration Center for Earth System Sciences and Remote Sensing; jhrisko000@citymail.cuny.edu, pramamurthy@ccny.cuny.edu*
[2] *National Oceanic and Atmospheric Administration; yunyue.yu@noaa.gov, peng.yu@noaa.gov*

Abstract

An urban air temperature model is presented using the enterprise GOES-16 land surface temperature product. The model is constructed by fitting the difference between ground-truth air temperature data against satellite LST using a Gaussian function. A time-match algorithm aligns the ground and satellite measurements within 5-minutes of one another, and the resulting matched values are compared over ten months to investigate their correlation. Land cover, latitude, longitude, local time, and elevation are input to a regressive neural network to fit each unique GOES-16 pixel according to ground-based properties. Over 150 ground stations and satellite pixels throughout the continental U.S. are used near urban areas to construct the diurnal Gaussian relationship and approximate air temperature. Statistics from a five month validation period generates an RMSE of 2.6 K, a bias of 0.8 K, and R^2 of 0.86, which are in strong competition with other studies at lower resolution, less geographic integration, and less temporal resolvability. The algorithm also produced strong spatial correlations with a high resolution numerical model, resulting in a mean RMSE value of 2.1 K for nearly 7,000 pixels. The overall presentation of this model aims to simplify the calculation of air temperature from satellite LST and create a successful model that performs well in heterogeneous environments. The improvement of urban air temperature calculations will also result in improved satellite land surface products such as relative humidity and heat index.

Keywords: Air Temperature, GOES-16, Neural Network, Regression, LST, Air Temperature Model, Satellite Remote Sensing

---

1. Introduction and Background

Spatial air temperature fluctuations can span 7 - 9 K in urban areas where land cover is highly heterogeneous (Eliasson and Svensson, 2003; Yan et al., 2014b). As a result, low-resolution forecasts and ground station networks can misrepresent air temperature distributions in regions where micro-scale variations are significant (Muller et al., 2013; Yan et al., 2014a). Moreover, fine-scale urban weather models require large computational resources or lengthy run times, neither of which are ideal in extreme weather scenarios (Chen et al., 2011; Mauree et al., 2018). These shortcomings reinforce the need for higher temporal resolution remote sensing tools for weather and public health applications in cities, where the majority of humans live (Kadhim et al., 2016; United Nations, 2014).

In recent years, weather and climate research has refocused its efforts on understanding the impacts of urbanization (Kloog et al., 2014; Krishnan et al., 2015; Li et al., 2018b; Pichierri et al., 2012). Much of the progress centers on single-city or regional analyses, which do not fully uncover the influence of urbanization on variables such as temperature and humidity. For the research that has been conducted on country-wide or continental scales, the exploration of temperature variability, as an example, is often limited to daily averages or daily maxima and minima rather than complete diurnal profiles (Good, 2015; Ho et al., 2014; Li et al., 2018a; Zhu et al., 2017). The lack of quality temporal and spatial data prevents proper algorithmic validation, which often happens when dealing with MODIS and Landsat, which are limited to two data points per day and a single point every 16 days, respectively (Cook et al., 2014; Wan, 2015).

These limitations were undoubtedly taken into account when developing the latest Geostationary Operational Environmental Satellite (GOES), GOES-16, which boasts 5-minute scan intervals and 2-km spatial granularity (Yu et al., 2016). With its high temporal resolution, GOES-16 is already being utilized for testing and development of ready-to-use products like sea surface temperature (Castro et al., 2018; Nardelli et al., 2015; Petrenko et al., 2011) and aerosol estimates (Hoff et al., 2014). However, other important near-surface measures like air temperature and humidity remain mostly unexplored, despite their correlation to debilitating urban heat island (UHI) effects (Jin, 2012). And since UHI has been well-documented as a catalyst for increased death tolls due to extreme heat (Tan et al., 2010; Zhao et al., 2014), it is the driving force behind the need for an accurate and robust air temperature algorithm.

Beyond applications with GOES-16, numerous studies have developed near-surface air temperature, T_{air}, algorithms built around remote sensing tools (Benali et al., 2012; Nieto et al., 2011; Sun et al., 2005). For the abun-

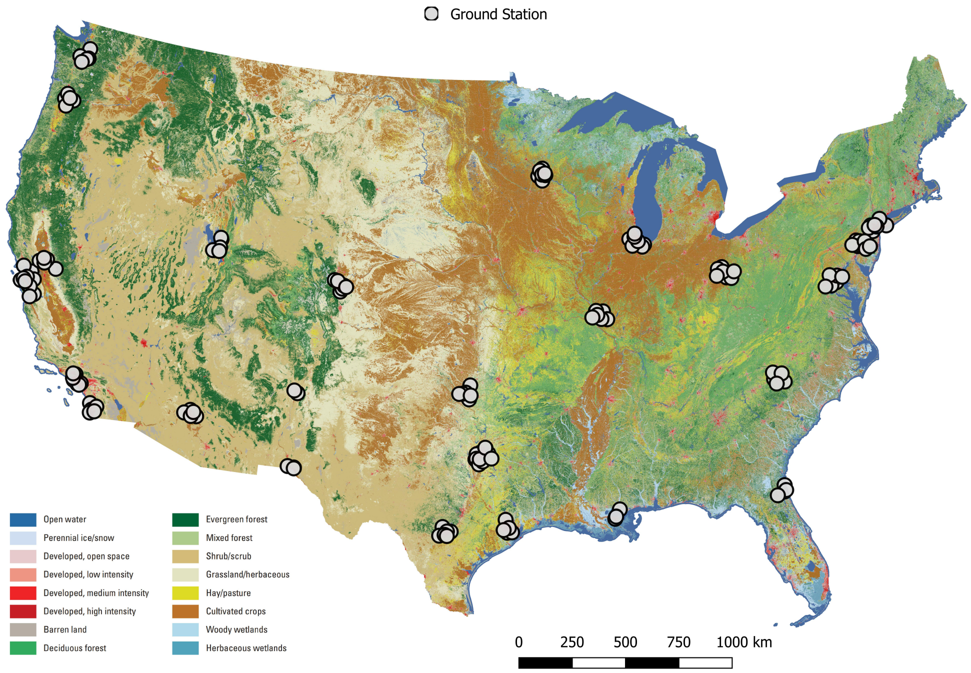

Figure 1: Ground station distribution atop the National Land Cover Database (NLCD) in the continental United States. Each group of points is centered around an urban area where each pointfalls within 50-km of the center of the corresponding city. The NLCD land cover classes, ground station elevation and latitude and longitude will be used as inputs to the air temperature algorithm.

dance of studies available, many are urban-specific and employ both statistical and physical methodologies (Bechtel et al., 2017; Cristóbal et al., 2008; Hu et al., 2015; Schuch et al., 2017; Tsin et al., 2016). And while a majority of the analyses use linear and non-linear regression (Fabiola Flores and Lillo, 2010; Florio et al., 2004; Fung et al., 2009; Golkar et al., 2018; Janatian et al., 2017), other more contemporary techniques like kriging and machine learning have been validated and tested for urban sites (Jang et al., 2004; Mao et al., 2008; Marzban et al., 2018; Szymanowski et al., 2013). Many of the studies also incorporate multiple variables such as the normalized difference vegetation index (NDVI), land cover properties, total precipitable water (TPW), solar zenith angle, etc. to increase the correlation between satellite observations and ground processes (Hengl et al., 2012; Hu and Brunsell, 2015).

Following a thorough review of the relevant studies above (14 in total), ranges of root mean square error (RMSE) and mean absolute error (MAE) estimates have been established for benchmarking the success of an accurate urban air temperature model (Chai and Draxler, 2014). The range of observed RMSE values spans 2-3K on average, and the average range of MAE is slightly smaller with 1.8-2.8K. For each city used in this study, the average diurnal air temperature range is 14K, establishing an expected daily error of 13% - 21%. The lower limits are treated as the performance metrics for the algorithm developed in this study. And while no comprehensive satellite-derived T_{air} performance metric exists - the average ranges can establish bounds for a new algorithm derived using the GOES-16 satellite.

In this study, several new techniques correlating land surface temperature (LST) and air temperature are introduced. A novel, Gaussian, diurnal fit between LST and T_{air} is proposed. And while others have applied diurnal fits to LST with sine and spline curves, this is the first to do so with a Gaussian function (Gholamnia et al., 2017; Stisen et al., 2007). Furthermore, to expand the study to a country-wide scale, a neural network is invoked to expose the relationship between complex terrain, LST, and T_{air}. Gaussian constants are identified for each city by incorporating the National Land Cover Database (NLCD), geographic coordinates, elevation, and time of day into the neural network. The goal is to decouple geography and urbanization from LST to more accurately predict air temperature (Bechtel et al., 2014; Rendón et al., 2014; Zhang et al., 2011a).

In the next section, methods for acquiring data will be discussed using three resources: the GOES-16 satellite, the Automated Surface Observing System (ASOS), and the numerical Weather Research and Forecasting (WRF) model. The following section describes in detail the methodology associated with correlating LST to T_{air} and utilizing local and land cover properties for incorporation into the neural network. Then, the results will be introduced with training and independence tests between the satellite algorithm, ground observations, and numerical model. Lastly, a discussion and concluding section will help clarify whether the following research goals were attained:

1. Develop an air temperature model that can recreate diurnal temperature profiles in urban areas using GOES-16 Land Surface Temperature (LST)
2. Ensure geographic universality for cities across the U.S. by employing the National Land Cover Database (NLCD)
3. Compare the algorithm to a state-of-the-art numerical urban climate model

Part of the concluding section will also discuss the future of this work and potential urban applications. With the goals laid out above, a satellite-derived air temperature product will help bridge the gap between the sparse ground-based micro-networks, and large-scale weather models, which will improve upon the air temperature models currently in the literature, and create a product that can be used in all cities.

2. Data

2.1. Ground Stations

The Automated Surface Observing System (ASOS) was used to ground-truth T_{air} data for training and validation of the LST algorithm. The Iowa Environmental Mesonet (IEM) houses a complete historic database of 1-hour ASOS data, making it easy to download and use air temperature data for comparison. ASOS also gives sky conditions for each station, meaning clear-sky days are easy to identify for accurate correlation between ground data and corresponding clear GOES-16 data.

Ground stations were selected based on a 50-km radius drawn from the center of each city (based on the city's shapefile boundary). In total, 206 ASOS stations from 26 cities across the continental United States were used to establish geographic coordinates and identify nearby satellite pixels. Figure 1 shows the distribution of ground stations across the continental United States. The ten most populated cities were selected first, followed by 16 other cities with varying geography and elevation. The stations differed in latitude, longitude, elevation, land cover, and population.

The land cover-specific properties for each satellite pixel were classified using the NLCD, while a digital elevation model and geographic coordinates were selected as point data from each ground station. The model, therefore, relies heavily on the land cover distribution within each satellite pixel rather than ground station point. This was done with the intention of capturing land cover effects on the 2km satellite pixel that may not affect the ground station. These properties were recorded with the intention of detrending the relationship between satellite LST and ground air temperature using a diurnal regressive neural network.

The ASOS were recorded for ten months: five months dedicated to training and five months dedicated to validation. The specific periods dedicated were: January 1, 2018 - May 31, 2018 for the training, and July 1, 2018 - November 30, 2018 for the validation. June 2018 data were skipped due to issues in GOES-16 data. Each station was required to have at least three points per hour for the training and validation periods, reducing the total number of stations to 162 for the complete analysis.

2.2. National Land Cover Database (NLCD)

The NLCD 2011 was used to characterize each GOES-16 satellite pixel into 16 land cover classes (NLCD contains 20 classes in total, but four are Alaska-specific) (Wickham et al., 2014). The land cover classes are weighted as percentages for each satellite pixel such that each pixel carries an array of ground properties, and since the NLCD has a resolution of 30-m and GOES-16 has a resolution of 2-km, we have over 4000 values that are weighted for each satellite pixel. This was done with the intention of expanding the database used by the neural network, which proves essential for increased performance from the air temperature model.

2.3. GOES-16 Satellite

The GOES-16 Enterprise Land Surface Temperature (LST) product is delivered at 5-minute intervals, allowing high temporal resolution comparison against ground-truth air temperature. The LST is calculated using IR bands 14 (11.2 µm) and 15 (12.3 µm), and a daily split-window channel emissivity developed by the Land Surface Temperature Algorithm Working Group at NOAA. The enterprise LST product differs from the official baseline LST in temporal resolution (5-min vs 1-hour). The algorithm is being developed for multiple sensors, the first being the Visible Infrared Imaging Radiometer Suite (VIIRS), and will be publicly available on the GOES-16 Advanced Baseline Imager (ABI) in the future (Yu et al., 2017). Currently, the implementation into the GOES-16 satellite is only available to our team.

The enterprise algorithm narrows the temporal comparison window between satellite LST and ground air temperature down to 2.5 minutes (compared to the usual 30 minutes). The LST product also has a spatial resolution of 2-km, meaning that most of the ground stations were delegated a unique satellite pixel for testing and validation of the algorithm. The GOES-16 product is designed to have an accuracy below 2.5 K, however, the accuracy and precision will be essential for statistical prediction of the air temperature algorithm development. For the case study of VIIRS - errors spanned 0.3 K - 0.9 K, which indicates the absolute minimum accuracy of the potential air temperature algorithm.

2.4. Urbanized Weather Research and Forecasting Model

The Weather Research and Forecasting (WRF version 3.9.9.1) model (Skamarock and Coauthors, 2008) initialized with the North American Mesoscale (NAM) forecast was run from June 14 - Jun 16, 2018. The model configuration utilizes three domains centered over New York City with domain resolutions of 9-km (120x120), 3-km (121x121), and 1-km (85x82). There are 51 vertical levels, with the first level at 10-m and a total of 30 levels below 1000-m intended to resolve the atmospheric boundary layer.

For the radiation schemes, the Dudhia scheme (Dudhia, 1989) is used for shortwave, and the Rapid Radiative Transfer Model is used for the longwave (Mlawer et al., 1997). Only the two coarser domains run the Kain-Fritsch cumulus parameterization (Kain, 2004), and only the 1-km domain uses microphysics, for which the WRF Single-moment 6-class scheme was selected. For the land surface model, the NOAH scheme was used (Tewari et al., 2016). The Mellor-Yamada-Janjic and the Eta Similarity schemes (Janjić, 1994) were used for the boundary layer and surface layer schemes, respectively.

The large number of levels in the boundary-layer helps to better represent the building-atmosphere interaction within a multi-layer urban canopy framework developed by (Martilli et al., 2002). The coupled Building Environment Parameterization (BEP) and Building Energy Model (BEM) (Salamanca and Martilli, 2009) parameterize the urban surface exchanges. Additionally, a cooling tower was added to the BEM parameterization to account for the latent heat released from buildings (Gutierrez et al., 2015). For the urban grids in New York City, the Primary Land Use Tax Lot Output (PLUTO), was used to define the urban morphology parameters of building area fraction, building surface area-to-height ratio, and building heights according to (Gutiérrez et al., 2015). The PLUTO data has been aggregated from its tax-lot based resolution to 1-km aggregates for the fine resolution domain. Accounting for the mechanical and thermal effects of buildings has also resulted in more accurate estimates of urban temperature and winds (Gutiérrez et al., 2015).

3. Algorithms and Data Training

3.1. Relationship Between LST and Air Temperature

The relationship between satellite LST and 2-m air temperature has been observed and quantified in several remote sensing and environmental studies (Gallo et al., 2011; Mutiibwa et al., 2015; Shen and G Leptoukh, 2011). For the current analysis, a robust correlation between the 162 ground stations and their corresponding nearby LST value is established using the GOES-16 satellite. The five-month averaged training profiles (Jan - May, 2018) for each of the 162 stations is shown in Fig. 2. These difference plots indicate a clear diurnal profile, which was crucial for establishing a general relationship between ground and satellite data.

A Gaussian function was chosen to fit the profiles in Fig. 2 and resulted in the best overall performance for all 162 stations. The overall error in the averaged diurnal plots indicate a minimum absolute error for the algorithm of 1.65 K. This value marks the minimum achievable error between our satellite air temperature algorithm and the ground station true air temperature. And since this value is below almost every study in the literature, a decision was made to continue with this method of analysis under the hypothesis that the application has the potential to outperform other models.

3.2. Diurnal Gaussian Fit

The Gaussian fit was chosen based on its similarity to the profile observed in the diurnal difference between air temperature and satellite LST. It is also

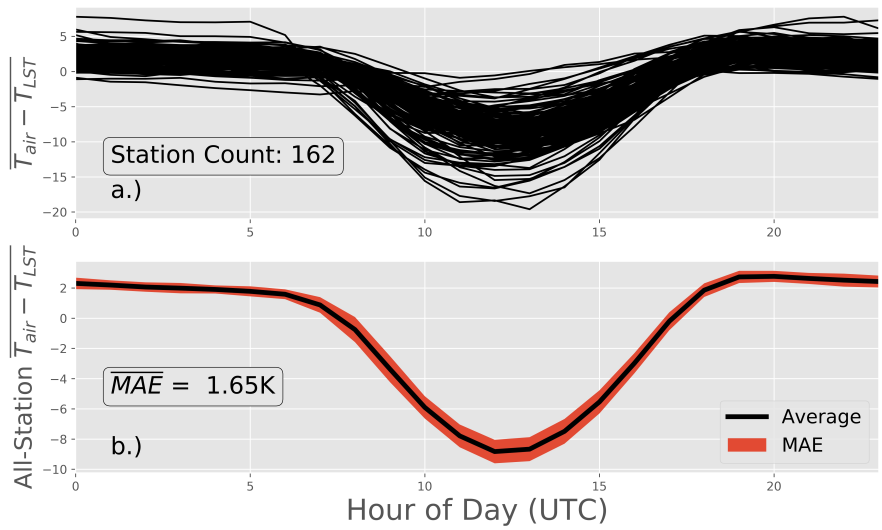

Figure 2: Hourly-averaged difference between ground station air temperature and the nearest GOES-16 LST pixel. The hourly averages have been computed for five months of training data, which includes 162 stations across the continental U.S.A. in 26 cities. The mean absolute error for the averages is 1.65K, indicating the lower limit on the possible performance for the diurnal model.

a novel choice, as many choose either sinusoidal, linear, or spline fits when correlating the two measurements (Zhou et al., 2013). Since the Gaussian fit was chosen over the other methods, it also requires a total of four constants as part of its input. In our case, we use the satellite LST and time-of-day (UTC) as input variables, which leads to our final modeling equation:

$$T_{air} = T_{LST} + y_0 - A_0 e^{\frac{(t-t_p)^2}{2\sigma^2}} \tag{1}$$

The four parameters, y_0, A_0, t_p, and σ are all found using properties of the GOES-16 pixel and air temperature elevation (the ground station in this case). Each of the parameters in the Gaussian fit can be thought of as different warpings due to station and geographic location. T_{LST} is the GOES-16 land surface temperature at the nearest pixel to the ground station (within 5-minutes from the ground station), t is the time-of-day input with units of hours, t_p is a time-of-day peak shift parameter with units of hours, σ is a Gaussian width parameter with units of hours, y_0 is a shift parameterwith units of Kelvin, and A_0 is an amplitude parameter with units of Kelvin.

The Gaussian was fitted using a method similar to that mentioned in (Guo, 2011) and (Bonham-Carter, 1988), where the exponential function is used to maximize the correlation between the Gaussian function and the diurnal difference between LST and T_{air}. Using a non-linear least-squares method, each ground station produced a series of parameters from each fit, which were then input to a database consisting of four parameters for each of the 162 ground station points. This array of 162 by 4 will later be used in the regressive neural network to find a relationship between the land cover, latitude, longitude, and elevation and each of the four constants in the Gaussian fit.

3.3. Regressive Neural Network

A regressive neural network was used to identify and weight the influence of land cover, elevation, latitude, and longitude such that unique expressions can be established for all four Gaussian constants based on the local landscape (Mas and Flores, 2008). The neural network is capable of looping through each of the 19 local parameters (16 NLCD classes, elevation, latitude, longitude) and quantifying the dependence of each on the Gaussian constants. Below is an implementation of the coefficients on each local

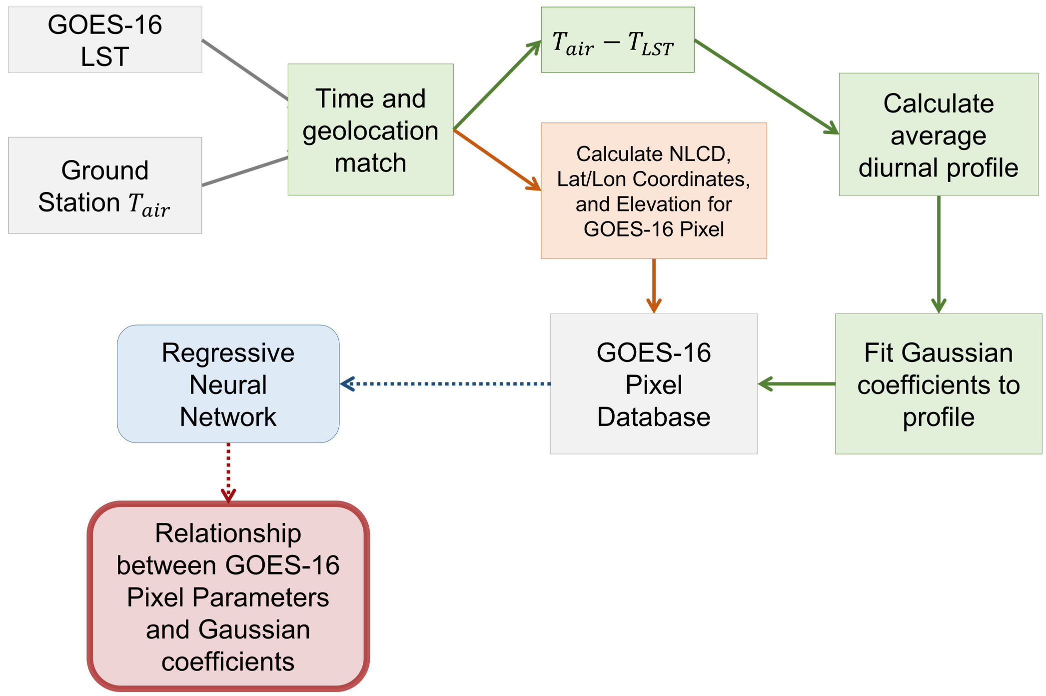

Figure 3: Flow diagram for calculating air temperature from GOES-16 land surface temperature (LST) using a diurnal Gaussian model and a regressive neural network.

parameter:

$$y_0, A_0, t_p, \sigma \underset{j}{\;} = \sum_{k=0}^{N=18} C_{j,k} p_{i,j,k} + D_{j,k} \tag{2}$$

where j is the index of the Gaussian parameter (0 is y_0, 1 is A_0, 2 is t_p, and 3 is σ). The i indicates a specific station, $C_{j,k}, D_{j,k}$ represent the universal constants for the model which are looped over a specific Gaussian parameter and pixel-specific index (k), and $p_{i,j,k}$ signifies which value to use based on index of Gaussian parameter, station, and pixel-specific index.

4. Results

4.1. Air Temperature Model Performance Against Ground Stations

For testing of the regressive neural network performance, 162 different GOES-16 pixels in 26 cities were used to create a database containing coefficients for each respective diurnal Gaussian curve. The database was used to train the regressive neural network which established relationships between satellite land surface temperature (LST) and ground station air temperature (T_{air}). The study trained over five months (January 1, 2018 - May 31, 2018) of data, with the ground station acting as the latitude and longitude location and the nearest GOES-16 pixel as the comparison point. Four statistical variables were calculated: coefficient of determination (R^2), root-mean-square error (RMSE), mean-absolute error (MAE), and mean bias (Bias). The statistical measures are defined and used as follows:

$$R^2 = 1 - \frac{\sum_i (T_{i,model} - \overline{T_{air}})^2}{\sum_i (T_{i,air} - \overline{T_{air}})^2} \tag{3}$$

$$\text{RMSE} = \sqrt{\frac{1}{N}\sum_{i=1}^{N}(T_{i,model} - T_{i,air})^2} \tag{4}$$

$$\text{MAE} = \frac{1}{N}\sum_{i=1}^{N}|T_{i,model} - T_{i,air}| \tag{5}$$

$$\text{Bias} = \frac{1}{N}\sum_{i=1}^{N}(T_{i,model} - T_{i,air}) \tag{6}$$

For each station, the four statistical measures were calculated as general performance metrics. Overall, for 162 stations, the statistical outcomes were

Table 1: Average model performance statistics against ground station data for the training period (Jan. - May) and validation period (July - Nov.)

Dates (2018)	Stations	# Points	R^2	RMSE	MAE	Bias
Jan. 1 - May 31	162	1284	0.90	2.4	1.8	0.3
July 1 - Nov. 30	156	1617	0.86	2.6	2.2	0.8

calculated for both the five month training and five month validation periods. The statistical results of both periods can be found in Table 1.

As expected, we see a slight decrease in performance metrics for the validation period compared to the training period. The R^2 value is slightly lower from 0.9 to 0.86, the RMSE and MAE only increased by 0.2 K and 0.4 K, respectively. And the bias increased to 0.8 K from 0.3 K. It was thought that the increase in bias was due to seasonal dependence, however, reversing the training and validation periods did not produce a bias in the negative direction - indicating that seasonal dependence is likely not the cause. These results demonstrate very good agreement between the training and validation, as well as the stability of the algorithm over multiple seasons and large ranges in temperatures.

Figure 4 demonstrates the performance of the model for four urban sites across the country. The sites were chosen based on their urbanization, which is the sum of all four urban categories. The second criteria was based on the availability of consecutive clear periods, which we can see as smooth profiles. The selected days contain periods of dropped data, both as a result of satellite LST product quality filtering and unavailable ground station periods.

Several observations can be made regarding the diurnal profiles in Figure

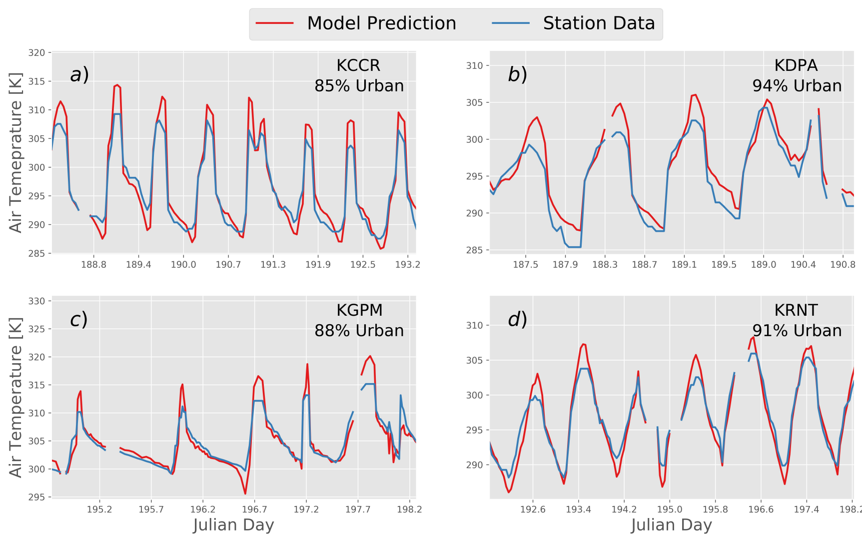

Figure 4: Diurnal reconstruction of air temperature from LST against ground stations for the validation period July - November 2018. Plot a) is from an urban station north east of San Francisco. Plot b) is from a Chicago station. Plot c) is from a station southwest of Dallas, and plot d) is from a Seattle-area station.

4. First, we can see marginal over-prediction during the daytime and under-prediction during the nighttime. This is likely due to the imperfect Gaussian fit applied to the diurnal profiles. We can also see the over-prediction in the average bias calculated in Table 1, which quantified the bias to be about 0.8 K.

An example of the scatter for three individual stations against their respective satellite predictions can be seen in Figure 5. The distribution of data can be observed as well-fitted to the one-to-one line, and this is true for multiple stations. There is also little-to-no temperature dependence on accuracy, which signifies great linearity between satellite algorithm and ground-truth

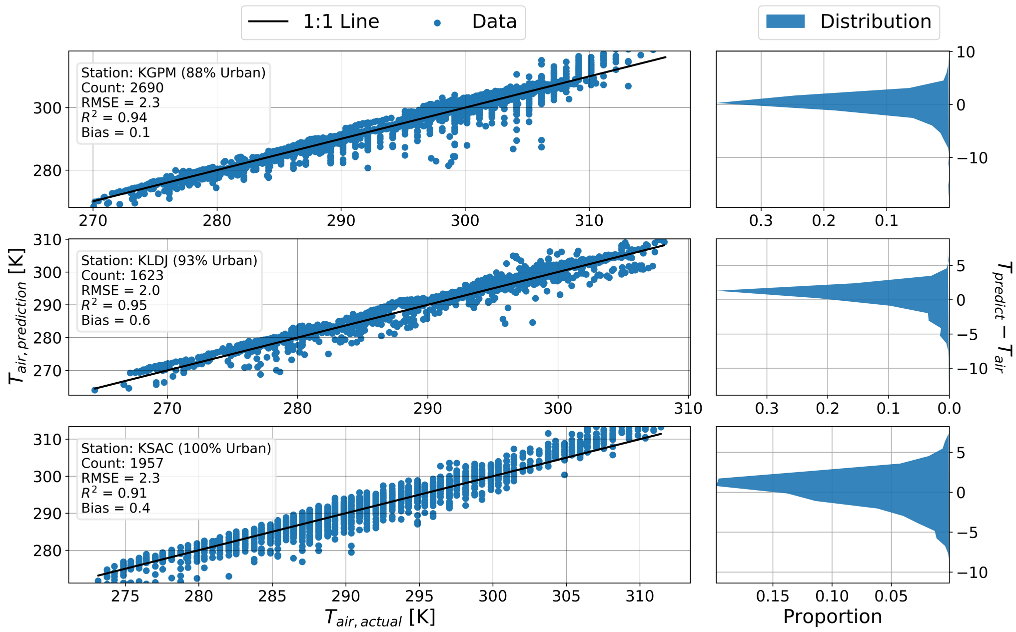

Figure 5: Scatter and difference plots for ground station and satellite-predicted air temperature for three individual stations in Dallas, TX (top), Elizabeth, NJ (middle), and Sacramento, CA (bottom). Each station is at least 70% urban. The scatter shows the adherence of the prediction algorithm to the true ground station temperatures. The distribution shows the distribution of the scatter.

station measurements. This high correlation also alludes to the likelihood that extreme heat events can be tracked without decrease in accuracy.

4.2. Satellite-Derived Air Temperature, Urban Weather Model, and Ground Station Comparison

The urbanized weather research and forecasting model (uWRF) was compared to ground stations in the same method as the GOES-16 satellite-derived air temperature. The nearest spatial pixel to a given ground station was used, and the closest temporal periods were compared (within 30-minutes). The testing was done from June 14 - Jun 16, 2018 for a test period of 72-hours. Six ground stations were selected for comparison in the New York City area (three in urban New Jersey and three in the New York boroughs).

The RMSE between the uWRF model and ground stations was found to be 1.6 K, while the RMSE between the satellite-derived air temperature and ground stations was approximated to be 2.1 K. Therefore, we can infer that the model outperforms the algorithm by 0.5 K for the test period and limited spatial domain. It should be noted that the uWRF model used here has representations for buildings and various urban processes, including heat and water vapor exhaust from ventilation systems, which is likely the reason for such strong performance. The model has also been specifically tailored for the New York City region. Three example stations comparing the air temperatures from all three methods (uWRF, satellite, ground station) can be seen in Figure 6.

Both air temperature models carry an inherent bias when compared to the ground stations, the uWRF bias is 0.1 K and the GOES-16 bias is 1.2 K. We saw the same bias above in the country-wide comparison between satellite air temperature and ground station. Another detail to note from Fig. 6 is the occurrence of dropped data. The dropped data phenomenon is likely due to cloud contamination, which occurs frequently during the summer in New York City during and just after peak heating. Therefore, some of the error associated with the satellite-derived model can be attributed to interchange periods between clear and cloudy skies.

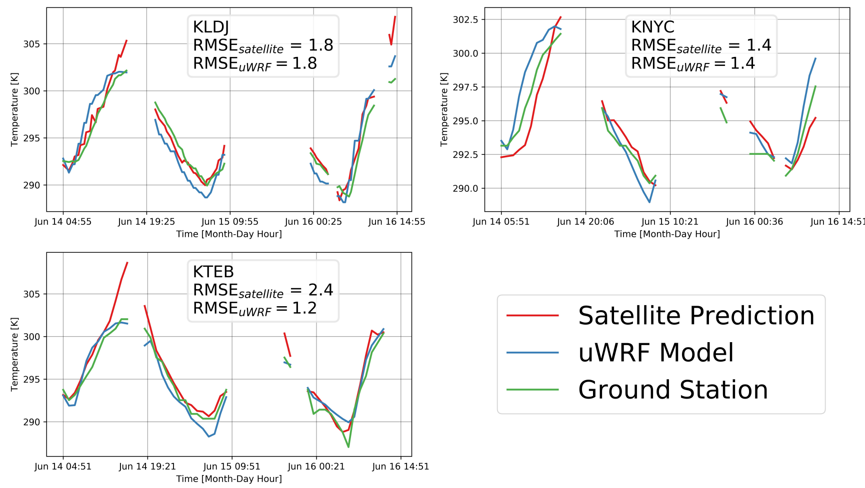

Figure 6: uWRF model 2-m air temperature output, GOES-16 air temperature prediction using LST, and ASOS ground station air temperature shown for three days in June 2018. The gaps in data represent dropped or unavailable data from either the satellite or ground station.

In the future, the biases and errors associated with the satellite model may be predictable and correctable , perhaps by introducing a higher resolution land surface temperature product via downscaling and cloud cover-specific prediction algorithms, however, those are tasks to be broached in a future work. In the next section, the ground stations will be omitted to facilitate a larger spatial correlation between uWRF predictions and satellite-derived air temperature can be further analyzed.

4.3. Spatial Distribution of Air Temperature

After verifying the correlation between ground stations, uWRF pixels, and satellite-derived air temperature, we can investigate the spatial correlation between uWRF and satellite pixels where ground stations do not exist. A 81x84 pixel grid resulted in roughly 6,804 pixels available for correlation between satellite and uWRF temperatures. This correlation downscales the satellite air temperature model from 2-km to 1-km to match the research forecasting model. An example snapshot of the difference between the GOES-16 prediction and the uWRF model can be seen in Figure 7.a. For the test period, the RMSE between the two methods was found to be 2.1 K, with the satellite-derived air temperature prediction having a bias of 1.1 K.

The correlation between the two is acceptable, considering there are spatial artifacts that can be observed such as incoming cloud contamination and dropped pixels. On very clear days, the RMSE ranges from 1.0 K to 1.5 K , indicating an even stronger correlation under ideal conditions. The low error between numerical model and LST-derived air temperature suggests that the model is portable and reliable for use as a high-resolution, efficient, accurate prediction of air temperature in cities across the United States.

Another example of the model's ability to recreate spatial maps is given in Fig. 7.b, where an independent snapshot was captured for a heat wave in New York City on August 28, 2018 during the peak temperature of the day. The plot in Figure 7.b shows the ability of the algorithm to capture pockets of heat, specifically in the more urban areas of the city. According to the LST-derived air temperature reproduction, temperatures in the city reached as high as 309 K during the daytime. And upon examination of weather records from that day, the maximum air temperature was found to be 308 K - meaning the algorithm could be used for citing extreme heat events and localization of hot spots in urban areas.

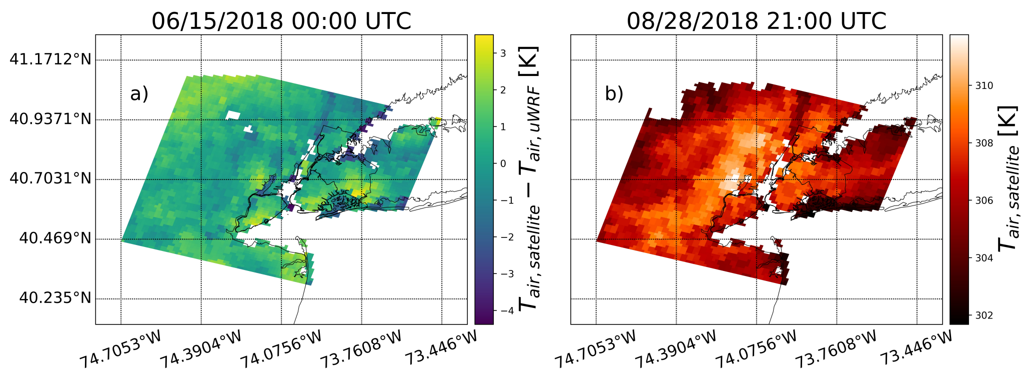

Figure 7: Plot a) shows a spatial comparison between satellite-predicted air temperature and WRF 2-m air temperature in plot. And plot b) shows spatial satellite-derived air temperature plot over the New York City area during a heat wave, showing the stability of the air temperature algorithm during an extreme heat event.

Something particular to note is that just in the New York area shown in Fig. 7 , satellite-derived air temperature variations span up to 14K, which likely indicates cloud contamination. This could be an issue during implementation of the algorithm and may need addressing in the future. For daytime peaks during the heat wave, neighboring pixels were observed to vary 0.2-0.5K on average, with standard deviations as high as 0.8K, which can be interpreted as neighboring pixels that can be as large as 1.3K. These variations can have huge implications on urban applications such as energy and health.

5. Discussion

5.1. Geospatial Inconsistencies

In Fig. 8, the spatial distribution of error between satellite-derived air temperature and ground station air temperature is mapped across the continental U.S. for each of the 156 urban ASOS stations. After an in-depth inspection of the errors, there does not appear to be any strong correlation between the input parameters (i.e. latitude, longitude, elevation, land cover) and the RMS errors ($R^2 < 0.1$ for each linear fit).

One weak correlation between error and input parameter is the elevation ($R^2 \approx 0.08$ for the linear fit between elevation and RMS). The scatter is large, but an increase in elevation can be observed to weakly increase the RMS error. A few publications in the literature state that the coupling between air temperature and LST gets weaker at higher elevations (Deng et al., 2018; Lin et al., 2016; Pepin et al., 2016), so this is one hypothesis for the weak correlation and higher RMS at higher elevations.

5.2. Comparison with Other Studies

The difficulty of comparing the current study against others is that no other research has developed a country-wide, urban, diurnal, satellite-based air temperature model at such a high resolution in space and time. As stated in the introduction, many studies have developed daily mean, minimum, and maximum air temperature models using satellite data (Cristóbal et al., 2008; Good, 2015; Ho et al., 2014; Li et al., 2018a; Shi et al., 2016; Zhu et al., 2017).

One such study by (Gholamnia et al., 2017) used a similar method for diurnal analysis and focused on the country of Iran. It validated its data against the same stations it trained (no independent spatial verification), and did not focus on urban areas. And while the average error found in that study was 2.1 K, a lower error than our study, it wasn't tested for independence in spatial variability. Another study by (Rhee and Im, 2014) conducted in South Korea showed that errors of daily mean temperature were still between 2-4 K, which it cited as not much of an improvement compared to competing studies. Other larger studies cite similar errors ranging from 1-4 K, which is in line with this study's observations (Mildrexler et al., 2011; Song and Park, 2014).

As for urban areas, most studies are concerned with using LST for quantifying urban heat island effects (Agathangelidis et al., 2016), and many focus on a single region or city (Nichol et al., 2009; Oswald et al., 2012). Moreover, for the studies that do handle LST and air temperature in urban areas, their methods are limited to linear relationships that are surely not portable between cities (Azevedo et al., 2016; Koenig and Hall, 2010; Shen and Leptoukh, 2011).

Lastly, spatial variability of air temperature is difficult to quantify in urban areas where heterogeneity dominates. However, it is likely that with the aid of ground station networks at higher resolution than the ASOS network, the error associated with satellite-derived air temperature will become even lower than quantified in this paper. Some studies have already tested various spatial algorithms, including complicated methods like kriging (Zhang et al., 2011b), but they carry errors as large as or larger than this study

(Monestiez et al., 2001), and typically omit urban-specific sites.

It is important to note that this is a unique algorithm and methodology based on the advantages of the GOES-16 high temporal resolution satellite. The algorithm competes with many of the partial studies that have been conducted on similar topics of urban air temperature derivations from satellite land surface temperature. It excels due to the temporal information gained from the satellite's resolution, which facilitated country-wide algorithm development for approximating the diurnal profile of air temperature in cities. The uniqueness and range of the algorithm makes it difficult to directly compare with other studies, however as a broad quantification - the algorithm can arguably compete with other studies and algorithms because of its simplicity.

5.3. Application Potential

The air temperature model could provide unique solutions for an array of problems impacting the urban environment. The air temperature model can play a critical role in understanding urban heat island issues. It will be able to predict thermal hotspots within cities and coupled to social-economic data (O'Neill et al., 2005; Petkova et al., 2016), it can be used to quantify social vulnerability of various neighborhoods. The model's ability to spatially resolve urban air temperature will be beneficial for urban planning and understanding intra-city temperature variability. The model can be used to forecast spatially resolved heat indices for various cities (Rosenthal et al., 2014).

Currently, single point observations and weather forecasts are used to predict heat index during extreme heat events. While single point measurements fail to represent spatial variability, modern forecasts from the National

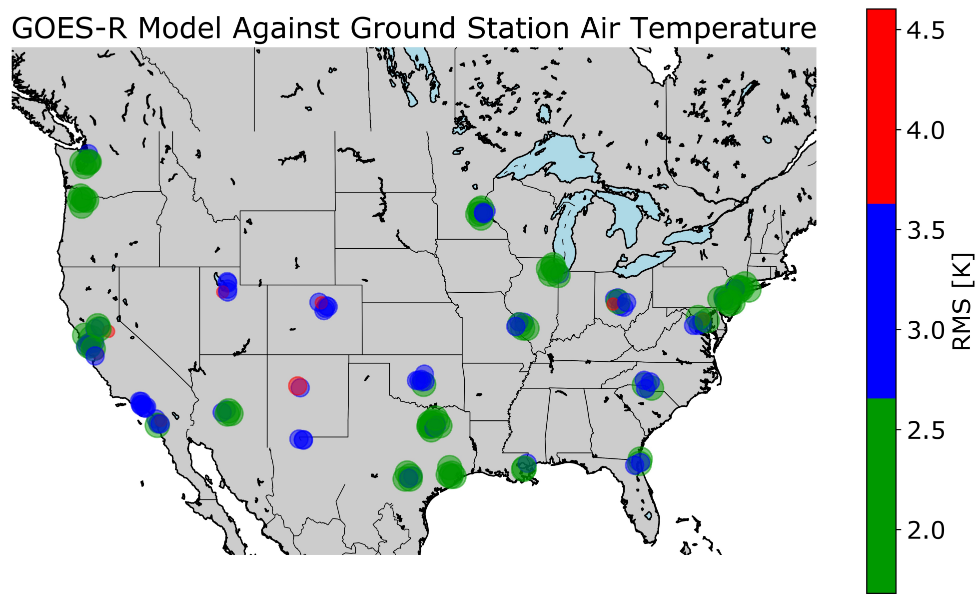

Figure 8: Overall error distribution for all 156 stations during the validation period from July - November 2018.

Weather Service also lack representation for urban areas. Hence, in the majority of cases, the urban heat index is mostly under predicted. Our model has the potential to create an accurate and cost-effective solution. We are currently working on a remote sensing-based model to calculate relative humidity for cities, which will hopefully improve the prediction of heat index in cities.

Another area where the model could be useful is in the field of urban energy use, distribution and power generation (Jones et al., 2015). Air temperature is well correlated with energy use and many models exploit this correlation to forecast energy demand that is vital for power generation (Krarti et al., 2017). Our model will be able to predict potential spatial variability in energy use. By coupling it to a building database, it could also predict vulnerable zones within the city. Ultimately the tool can be used to design smart distribution systems. The air temperature model can also be used to create a high resolution dataset to force urban climate models, which are increasingly used to study urban climate dynamics.

6. Conclusion

This research combined GOES-16 LST with land cover properties, geographic coordinates, elevation information, and time-of-day to create a robust Gaussian approximation of 2-m air temperature. The coefficients for each satellite pixel were derived using a regressive neural network and comparison against true air temperature at ground stations across the U.S. The performance of the GOES-16 air temperature model was further validated by comparison with a numerical WRF model, indicating agreement and performance between the satellite air temperature model and numerical 2-m air temperature.

The average RMSE between satellite-derived and measured 2-m air temperature was found to be 2.6 K for 156 pixels across 26 different cities in the continental United States (see Fig. 8 for the geospatial distribution of error). When comparing the algorithm to the numerical model, a RMSE of 2.1 K was calculated for nearly 7k pixels over a three day period during the summer of 2018. For very clear days, the RMSE decreased to as low as 1.0 K, indicating a strong correlation and great performance of the satellite-derived air temperature against the numerical 2-m air temperature. The algorithm shows great promise for improving the current air temperatures in cities, as they are often reliant on lower-resolution numerical models or single-point observations. This algorithm is the first step toward a possible heat index product - a parameter that is essential for marking extreme heat events, specifically in urban areas where death tolls can rise beyond the surrounding areas.

Acknowledgements

This study is supported and monitored by The National Oceanic and Atmospheric Administration – Cooperative Science Center for Earth System Sciences and Remote Sensing Technologies (NOAA-CESSRST) under the Cooperative Agreement Grant #: NA16SEC4810008. The authors would like to thank The City College of New York, NOAA-CESSRST (aka CREST) program and NOAA Office of Education, Educational Partnership Program for full fellowship support for Joshua Hrisko. The statements contained within the manuscript/research article are not the opinions of the funding agency or the U.S. government, but reflect the author's opinions. The research is also funded by The Department of Defense Army Research Office Grant # W911NF-18-1-0371. Computational resources were provided by the CUNY High Performance Computing Center, funded, in part, by grants from the City of New York, State of New York, CUNY Research Foundation, and National Science Foundation Grants CNS-0958379, CNS-0855217 and ACI 1126113.

References

Agathangelidis, I., Cartalis, C., Santamouris, M., 2016. Estimation of air temperatures for the urban agglomeration of Athens with the use of satellite data. Geoinformatics & Geostatistics: An Overview 4. doi:10.4172/2327-4581.1000139.

Azevedo, J.A., Chapman, L., Muller, C.L., 2016. Quantifying the daytime and night-time urban heat island in Birmingham, UK: A comparison of satellite derived land surface temperature and high resolution air temperature observations. Remote Sensing 8. http://www.mdpi.com/2072-4292/8/2/153, doi:10.3390/rs8020153.

Bechtel, B., Wiesner, S., Zakšek, K., 2014. Estimation of dense time series of urban air temperatures from multitemporal geostationary satellite data. IEEE Journal of Selected Topics in Applied Earth Observations and Remote Sensing 7, 4129–4137. doi:10.1109/JSTARS.2014.2322449.

Bechtel, B., Zakšek, K., Oßenbrügge, J., Kaveckis, G., Böhner, J., 2017. Towards a satellite based monitoring of urban air temperatures. Sustainable Cities and Society 34, 22 – 31. http://www.sciencedirect.com/science/article/pii/S2210670716307569.

Benali, A., Carvalho, A., Nunes, J., Carvalhais, N., Santos, A., 2012. Estimating air surface temperature in Portugal using MODIS LST data. Remote Sensing of Environment 124, 108 – 121. http://www.sciencedirect.com/science/article/pii/S0034425712002003.

Bonham-Carter, G., 1988. Numerical procedures and computer program for fitting an inverted gaussian model to vegetation reflectance data. Computers & Geosciences 14, 339 – 356. http://www.sciencedirect.com/science/article/pii/0098300488900659.

Castro, S.L., Monzon, L.A., Wick, G.A., Lewis, R.D., Beylkin, G., 2018. Subpixel variability and quality assessment of satellite sea surface temperature data using a novel high resolution multistage spectral interpolation (HRMSI) technique. Remote Sensing of Environment 217, 292 – 308. http://www.sciencedirect.com/science/article/pii/S003442571830395X.

Chai, T., Draxler, R.R., 2014. Root mean square error (RMSE) or mean absolute error (MAE)?- arguments against avoiding RMSE in the literature. Geoscientific Model Development 7, 1247–1250. https://www.geosci-model-dev.net/7/1247/2014/.

Chen, F., Kusaka, H., Bornstein, R., Ching, J., Grimmond, C.S.B., Grossman-Clarke, S., Loridan, T., Manning, K.W., Martilli, A., Miao, S., Sailor, D., Salamanca, F.P., Taha, H., Tewari, M., Wang, X., Wyszogrodzki, A.A., Zhang, C., 2011. The integrated WRF/urban modelling system: development, evaluation, and applications to urban environmental problems. International Journal of Climatology 31, 273–288. https://rmets.onlinelibrary.wiley.com/doi/abs/10.1002/joc.2158.

Cook, M., Schott, J.R., Mandel, J., Raqueno, N., 2014. Development of an operational calibration methodology for the landsat thermal data archive and initial testing of the atmospheric compensation component of a land surface temperature (LST) product from the archive. Remote Sensing 6, 11244–11266. http://www.mdpi.com/2072-4292/6/11/11244.

Cristóbal, J., Ninyerola, M., Pons, X., 2008. Modeling air temperature through a combination of remote sensing and GIS data. Journal of Geophysical Research: Atmospheres 113. https://agupubs.onlinelibrary.wiley.com/doi/abs/10.1029/2007JD009318.

Deng, Y., Wang, S., Bai, X., Tian, Y., Wu, L., Xiao, J., Chen, F., Qian, Q., 2018. Relationship among land surface temperature and LUCC, NDVI in typical karst area. Scientific Reports 8, 1–12. doi:10.1038/s41598-017-19088-x.

Dudhia, J., 1989. Numerical study of convection observed during the winter monsoon experiment using a mesoscale two-dimensional model. Journal of the Atmospheric Sciences 46, 3077–3107. https://doi.org/10.1175/1520-0469(1989)046<3077:NSOCOD>2.0.CO;2.

Eliasson, I., Svensson, M.K., 2003. Spatial air temperature variations and urban land use — a statistical approach. Meteorological Applications 10, 135–149. https://rmets.onlinelibrary.wiley.com/doi/abs/10.1017/S1350482703002056.

Fabiola Flores, P., Lillo, M., 2010. Simple air temperature estimation method from MODIS satellite images on a regional scale. Chilean Journal of Agricultural Research 70, 436–445.

Florio, E.N., Lele, S.R., Chang, Y.C., Sterner, R., Glass, G.E., 2004. Integrating AVHRR satellite data and NOAA ground observations to predict surface air temperature: a statistical approach. International Journal of Remote Sensing 25, 2979–2994. https://doi.org/10.1080/01431160310001624593.

Fung, W.Y., Lam, K.S., Nichol, J., Wong, M.S., 2009. Derivation of nighttime urban air temperatures using a satellite thermal image. Journal of Applied Meteorology and Climatology 48, 863–872. https://doi.org/10.1175/2008JAMC2001.1.

Gallo, K., Hale, R., Tarpley, D., Yu, Y., 2011. Evaluation of the relationship between air and land surface temperature under clear- and cloudy-sky conditions. Journal of Applied Meteorology and Climatology 50, 767–775. https://doi.org/10.1175/2010JAMC2460.1.

Gholamnia, M., Alavipanah, S.K., Darvishi Boloorani, A., Hamzeh, S., Kiavarz, M., 2017. Diurnal air temperature modeling based on the land surface temperature. Remote Sensing 9. http://www.mdpi.com/2072-4292/9/9/915.

Golkar, F., Sabziparvar, A.A., Khanbilvardi, R., Nazemosadat, M.J., Zand-Parsa, S., Rezaei, Y., 2018. Estimation of instantaneous air temperature using remote sensing data. International Journal of Remote Sensing 39, 258–275. https://doi.org/10.1080/01431161.2017.1382743.

Good, E., 2015. Daily minimum and maximum surface air temperatures from geostationary satellite data. Journal of Geophysical Research: Atmospheres 120, 2306–2324. https://agupubs.onlinelibrary.wiley.com/doi/abs/10.1002/2014JD022438.

Guo, H., 2011. A simple algorithm for fitting a gaussian function [DSP tips and tricks]. IEEE Signal Processing Magazine - IEEE SIGNAL PROCESS MAG 28, 134–137. doi:10.1109/MSP.2011.941846.

Gutierrez, E., Gonzalez, J., Martilli, A., Bornstein, R., 2015. On the anthropogenic heat fluxes using an air conditioning evaporative cooling parameterization for mesoscale urban canopy models. Journal of Solar Energy Engineering 137, 1–13. doi:10.1115/1.4030854.

Gutiérrez, E., Martilli, A., Santiago, J.L., González, J.E., 2015. A mechanical drag coefficient formulation and urban canopy parameter assimilation technique for complex urban environments. Boundary-Layer Meteorology 157, 333–341. https://doi.org/10.1007/s10546-015-0051-7.

Gutiérrez, E., González, J.E., Martilli, A., Bornstein, R., Arend, M., 2015. Simulations of a heat-wave event in New York City using a multilayer urban parameterization. Journal of Applied Meteorology and Climatology 54, 283–301. https://doi.org/10.1175/JAMC-D-14-0028.1.

Hengl, T., Heuvelink, G.B.M., Perčec Tadić, M., Pebesma, E.J., 2012. Spatio-temporal prediction of daily temperatures using time-series of MODIS LST images. Theoretical and Applied Climatology 107, 265–277. https://doi.org/10.1007/s00704-011-0464-2.

Ho, H.C., Knudby, A., Sirovyak, P., Xu, Y., Hodul, M., Henderson, S.B., 2014. Mapping maximum urban air temperature on hot summer days. Remote Sensing of Environment 154, 38 – 45. http://www.sciencedirect.com/science/article/pii/S0034425714003095.

Hoff, R.M., Kondragunta, S., Ciren, P., Xu, C., Zhang, H., Huff, A., 2014. Development of synthetic GOES-R ABI aerosol products. Atmospheric Measurement Techniques Discussions 7, 10131–10157. https://www.atmos-meas-tech-discuss.net/7/10131/2014/.

Hu, L., Brunsell, N.A., 2015. A new perspective to assess the urban heat island through remotely sensed atmospheric profiles. Remote Sensing of Environment 158, 393 – 406. http://www.sciencedirect.com/science/article/pii/S0034425714004325.

Hu, L., Monaghan, A.J., Brunsell, N.A., 2015. Investigation of urban air temperature and humidity patterns during extreme heat conditions using satellite-derived data. Journal of Applied Meteorology and Climatology 54, 2245–2259. https://doi.org/10.1175/JAMC-D-15-0051.1.

Janatian, N., Sadeghi, M., Sanaeinejad, S.H., Bakhshian, E., Farid, A., Hasheminia, S.M., Ghazanfari, S., 2017. A statistical framework for estimating air temperature using MODIS land surface temperature data. International Journal of Climatology 37, 1181–1194. https://rmets.onlinelibrary.wiley.com/doi/abs/10.1002/joc.4766.

Jang, J.D., Viau, A.A., Anctil, F., 2004. Neural network estimation of air temperatures from AVHRR data. International Journal of Remote Sensing 25, 4541–4554. https://doi.org/10.1080/01431160310001657533.

Janjić, Z.I., 1994. The step-mountain eta coordinate model: Further developments of the convection, viscous sublayer, and turbulence closure schemes.

Monthly Weather Review 122, 927–945. https://doi.org/10.1175/1520-0493(1994)122<0927:TSMECM>2.0.CO;2.

Jin, M.S., 2012. Developing an index to measure urban heat island effect using satellite land skin temperature and land cover observations. Journal of Climate 25, 6193–6201. https://doi.org/10.1175/JCLI-D-11-00509.1.

Jones, R.V., Fuertes, A., Lomas, K.J., 2015. The socio-economic, dwelling and appliance related factors affecting electricity consumption in domestic buildings. Renewable and Sustainable Energy Reviews 43, 901 – 917. http://www.sciencedirect.com/science/article/pii/S1364032114010235.

Kadhim, N., Mourshed, M., Bray, M., 2016. Advances in remote sensing applications for urban sustainability. Euro-Mediterranean Journal for Environmental Integration 1, 7. https://doi.org/10.1007/s41207-016-0007-4.

Kain, J.S., 2004. The Kain-Fritsch convective parameterization: An update. Journal of Applied Meteorology 43, 170–181. https://doi.org/10.1175/1520-0450(2004)043<0170:TKCPAU>2.0.CO;2.

Kloog, I., Nordio, F., Coull, B.A., Schwartz, J., 2014. Predicting spatiotemporal mean air temperature using MODIS satellite surface temperature measurements across the northeastern usa. Remote Sensing of Environment 150, 132 – 139. http://www.sciencedirect.com/science/article/pii/S0034425714001758.

Koenig, L.S., Hall, D.K., 2010. Comparison of satellite, thermochron and air temperatures at Summit, Greenland, during the winter of 2008/09. Journal of Glaciology 56, 735–741. doi:10.3189/002214310793146269.

Krarti, A., Ortiz, L., Gonzalez, J., 2017. On the spatio-temporal end-user energy demands of a dense urban environment. Journal of Solar Energy Engineering 139. doi:10.1115/1.4036545.

Krishnan, P., Kochendorfer, J., Dumas, E.J., Guillevic, P.C., Baker, C.B., Meyers, T.P., Martos, B., 2015. Comparison of in-situ, aircraft, and satellite land surface temperature measurements over a NOAA climate reference network site. Remote Sensing of Environment 165, 249 – 264. http://www.sciencedirect.com/science/article/pii/S0034425715300109.

Li, X., Zhou, Y., Asrar, G.R., Zhu, Z., 2018a. Developing a 1km resolution daily air temperature dataset for urban and surrounding areas in the conterminous United States. Remote Sensing of Environment 215, 74 – 84. http://www.sciencedirect.com/science/article/pii/S0034425718302633.

Li, X., Zhou, Y., Zhu, Z., Liang, L., Yu, B., Cao, W., 2018b. Mapping annual urban dynamics (1985-2015) using time series of Landsat data. Remote Sensing of Environment 216, 674 – 683. http://www.sciencedirect.com/science/article/pii/S0034425718303638.

Lin, X., Zhang, W., Huang, Y., Sun, W., Han, P., Yu, L., Sun, F., 2016. Empirical estimation of near-surface air temperature in China from MODIS

LST data by considering physiographic features. Remote Sensing 8. doi:10.3390/rs8080629.

Mao, K.B., Tang, H.J., Wang, X.F., Zhou, Q.B., Wang, D.L., 2008. Near-surface air temperature estimation from replaced[id=r2]ASTER aster data based on neural network algorithm. International Journal of Remote Sensing 29, 6021–6028. https://doi.org/10.1080/01431160802192160.

Martilli, A., Clappier, A., Rotach, M.W., 2002. An urban surface exchange parameterisation for mesoscale models. Boundary-Layer Meteorology 104, 261–304. https://doi.org/10.1023/A:1016099921195.

Marzban, F., Conrad, T., Marzban, P., Sodoudi, S., 2018. Estimation of the near-surface air temperature during the day and nighttime from MODIS in Berlin, Germany. International Journal of Advanced Remote Sensing and GIS 7.

Mas, J.F., Flores, J.J., 2008. The application of artificial neural networks to the analysis of remotely sensed data. International Journal of Remote Sensing 29, 617–663. https://doi.org/10.1080/01431160701352154, doi:10.1080/01431160701352154.

Mauree, D., Blond, N., Clappier, A., 2018. Multi-scale modeling of the urban meteorology: Integration of a new canopy model in the WRF model. Urban Climate 26, 60 – 75. http://www.sciencedirect.com/science/article/pii/S2212095518301688.

Mildrexler, D.J., Zhao, M., Running, S.W., 2011. A global comparison between station air temperatures and MODIS land surface temperatures reveals the cooling role of forests. Journal of Geophysical Research: Biogeosciences 116, 1–15. https://agupubs.onlinelibrary.wiley.com/doi/abs/10.1029/2010JG001486.

Mlawer, E.J., Taubman, S.J., Brown, P.D., Iacono, M.J., Clough, S.A., 1997. Radiative transfer for inhomogeneous atmospheres: RRTM, a validated correlated-k model for the longwave. Journal of Geophysical Research: Atmospheres 102, 16663–16682. https://agupubs.onlinelibrary.wiley.com/doi/abs/10.1029/97JD00237.

Monestiez, P., Courault, D., Allard, D., Ruget, F., 2001. Spatial interpolation of air temperature using environmental context: Application to a crop model. Environmental and Ecological Statistics 8, 297–309. https://doi.org/10.1023/A:1012726317935.

Muller, C.L., Chapman, L., Grimmond, C.S.B., Young, D.T., Cai, X., 2013. Sensors and the city: a review of urban meteorological networks. International Journal of Climatology 33, 1585–1600. https://rmets.onlinelibrary.wiley.com/doi/abs/10.1002/joc.3678.

Mutiibwa, D., Strachan, S., Albright, T., 2015. Land surface temperature and surface air temperature in complex terrain. IEEE Journal of Selected Topics in Applied Earth Observations and Remote Sensing 8, 4762–4774.

Nardelli, B.B., Pisano, A., Tronconi, C., Santoleri, R., 2015. Evaluation of different covariance models for the operational interpolation of high resolution satellite sea surface temperature data over the Mediterranean

Sea. Remote Sensing of Environment 164, 334 – 343. http://www.sciencedirect.com/science/article/pii/S0034425715001674.

Nichol, J.E., Fung, W.Y., se Lam, K., Wong, M.S., 2009. Urban heat island diagnosis using ASTER satellite images and 'in situ' air temperature. Atmospheric Research 94, 276 – 284. http://www.sciencedirect.com/science/article/pii/S0169809509001781.

Nieto, H., Sandholt, I., Aguado, I., Chuvieco, E., Stisen, S., 2011. Air temperature estimation with MSG-SEVIRI data: Calibration and validation of the TVX algorithm for the Iberian Peninsula. Remote Sensing of Environment 115, 107 – 116. http://www.sciencedirect.com/science/article/pii/S0034425710002506.

O'Neill, M.S., Zanobetti, A., Schwartz, J., 2005. Disparities by race in heat-related mortality in four us cities: The role of air conditioning prevalence. Journal of Urban Health 82, 191–197. https://doi.org/10.1093/jurban/jti043.

Oswald, E.M., Rood, R.B., Zhang, K., Gronlund, C.J., O'Neill, M.S., White-Newsome, J.L., Brines, S.J., Brown, D.G., 2012. An investigation into the spatial variability of near-surface air temperatures in the Detroit, Michigan, metropolitan region. Journal of Applied Meteorology and Climatology 51, 1290–1304. https://doi.org/10.1175/JAMC-D-11-0127.1.

Pepin, N.C., Maeda, E.E., Williams, R., 2016. Use of remotely sensed land surface temperature as a proxy for air temperatures at high elevations: Findings from a 5000m elevational transect across Kilimanjaro. Journal of Geophysical Research: Atmospheres 121, 9998–10,015. doi:10.1002/2016JD025497.

Petkova, E., Vink, J., Horton, R., Gasparrini, A., A. Bader, D., D. Francis, J., Kinney, P., 2016. Towards more comprehensive projections of urban heat-related mortality: Estimates for New York City under multiple population, adaptation, and climate scenarios. Environmental Health Perspectives 125. doi:10.1289/EHP166.

Petrenko, B., Ignatov, A., Shabanov, N., Kihai, Y., 2011. Development and evaluation of sst algorithms for GOES-R ABI using MSG SEVIRI as a proxy. Remote Sensing of Environment 115, 3647 – 3658. http://www.sciencedirect.com/science/article/pii/S0034425711003300.

Pichierri, M., Bonafoni, S., Biondi, R., 2012. Satellite air temperature estimation for monitoring the canopy layer heat island of Milan. Remote Sensing of Environment 127, 130 – 138. http://www.sciencedirect.com/science/article/pii/S0034425712003446.

Rendón, A.M., Salazar, J.F., Palacio, C.A., Wirth, V., Brötz, B., 2014. Effects of urbanization on the temperature inversion breakup in a mountain valley with implications for air quality. Journal of Applied Meteorology and Climatology 53, 840–858. https://doi.org/10.1175/JAMC-D-13-0165.1.

Rhee, J., Im, J., 2014. Estimating high spatial resolution air temperature for regions with limited in situ data using MODIS products. Remote Sensing 6, 7360–7378. http://www.mdpi.com/2072-4292/6/8/7360.

Rosenthal, J.K., Kinney, P.L., Metzger, K.B., 2014. Intra-urban vulnerability to heat-related mortality in New York City, 1997–2006. Health & Place 30, 45 – 60. http://www.sciencedirect.com/science/article/pii/S1353829214001087.

Salamanca, F., Martilli, A., 2009. A new building energy model coupled with an urban canopy parameterization for urban climate simulations—part ii. validation with one dimension off-line simulations. Theoretical and Applied Climatology 99, 345. https://doi.org/10.1007/s00704-009-0143-8.

Schuch, F., Marpu, P., Masri, D., Afshari, A., 2017. Estimation of urban air temperature from a rural station using remotely sensed thermal infrared data. Energy Procedia 143, 519 – 525. http://www.sciencedirect.com/science/article/pii/S1876610217364846. leveraging Energy Technologies and Policy Options for Low Carbon Cities.

Shen, S., G Leptoukh, G., 2011. Estimation of surface air temperature over central and eastern Eurasia from MODIS land surface temperature. Environmental Research Letters 6, 045206. doi:10.1088/1748-9326/6/4/045206.

Shen, S., Leptoukh, G.G., 2011. Estimation of surface air temperature over central and eastern Eurasia from MODIS land surface temperature. Environmental Research Letters 6, 045206. https://doi.org/10.1088%2F1748-9326%2F6%2F4%2F045206.

Shi, L., Liu, P., Kloog, I., Lee, M., Kosheleva, A., Schwartz, J., 2016. Estimating daily air temperature across the southeastern United States using high-resolution satellite data: A statistical modeling study. Environmental Research 146, 51 – 58. http://www.sciencedirect.com/science/article/pii/S0013935115301663.

Skamarock, W.C., Coauthors, 2008. A description of the advanced research WRF version 3. Technical Report. NCAR. doi:10.5065/D68S4MVH. nCAR/TN-475+STR.

Song, B., Park, K., 2014. Validation of aster surface temperature data with in situ measurements to evaluate heat islands in complex urban areas. Advances in Meteorology 2014, 1–12. doi:10.1155/2014/620410.

Stisen, S., Sandholt, I., Nørgaard, A., Fensholt, R., Eklundh, L., 2007. Estimation of diurnal air temperature using MSG SEVIRI data in West Africa. Remote Sensing of Environment 110, 262 – 274. http://www.sciencedirect.com/science/article/pii/S0034425707000995.

Sun, Y.J., Wang, J.F., Zhang, R.H., Gillies, R.R., Xue, Y., Bo, Y.C., 2005. Air temperature retrieval from remote sensing data based on thermodynamics. Theoretical and Applied Climatology 80, 37–48. https://doi.org/10.1007/s00704-004-0079-y.

Szymanowski, M., Kryza, M., Spallek, W., 2013. Regression-based air temperature spatial prediction models: an example from Poland. Meteorologische Zeitschrift 22, 577–585. http://dx.doi.org/10.1127/0941-2948/2013/0440.

Tan, J., Zheng, Y., Tang, X., Guo, C., Li, L., Song, G., Zhen, X., Yuan, D., Kalkstein, A.J., Li, F., Chen, H., 2010. The urban heat island

and its impact on heat waves and human health in Shanghai. International Journal of Biometeorology 54, 75–84. https://doi.org/10.1007/s00484-009-0256-x.

Tewari, M., Chen, F., Wang, W., Dudhia, J., LeMone, M., Mitchell, K., Ek, M., Gayno, G., Wegiel, J., Cuenca, R., 2016. Implementation and verification of the united NOAH land surface model in the WRF model, in: 20th Conference on Weather Analysis and Forecasting/16th Conference on Numerical Weather Prediction, pp. 11–15.

Tsin, P.K., Knudby, A., Krayenhoff, E.S., Ho, H.C., Brauer, M., Henderson, S.B., 2016. Microscale mobile monitoring of urban air temperature. Urban Climate 18, 58 – 72. http://www.sciencedirect.com/science/article/pii/S221209551630044X.

United Nations, 2014. Department of Economic and Social Affairs Population Division. World urbanization prospects. https://www.un-ilibrary.org/content/publication/527e5125-en. The 2014 Revision, Highlights (ST/ESA/SER.A/352).

Wan, Z., H.S.H.G., 2015. MOD11 L2 MODIS/terra land surface temperature/emissivity 5-min L2 swath 1km V006 [data set]. https://doi.org/10.5067/MODIS/MOD11_L2.006. NASA EOSDIS LP DAAC.

Wickham, J., Homer, C., Vogelmann, J., McKerrow, A., Mueler, R., Herold, N., Coulston, J., 2014. The multi-resolution land characteristics (MRLC) consortium-20 years of development and integration of USA national land cover data. Remote Sensing 2014, 6, 7424-7441 6, 7424–7441.

Yan, H., Fan, S., Guo, C., Hu, J., Dong, L., 2014a. Quantifying the impact of land cover composition on intra-urban air temperature variations at a mid-latitude city. PLOS ONE 9, 1–10. https://doi.org/10.1371/journal.pone.0102124.

Yan, H., Fan, S., Guo, C., Wu, F., Zhang, N., Dong, L., 2014b. Assessing the effects of landscape design parameters on intra-urban air temperature variability: The case of Beijing, China. Building and Environment 76, 44 – 53. http://www.sciencedirect.com/science/article/pii/S0360132314000596.

Yu, Y., Liu, Y., Yu, P., Wang, H., 2017. Enterprise algorithm theoretical basis document for VIIRS land surface temperature production. https://www.star.nesdis.noaa.gov/jpss/documents/ATBD/ATBD_EPS_Land_LST_v1.0.pdf. NOAA.

Yu, Y., Yu, P., Rao, Y., 2016. Geostationary operational environmental satellite (GOES)-R series advanced baseline imager (ABI) L2+ land surface temperature (LST) beta, provisional, and full validation readiness, implementation, and management plan (RIMP). https://www.goes-r.gov/products/RIMPs/RIMP_ABI-L2_LST_v.1.0.pdf. NOAA STARR.

Zhang, D.L., Shou, Y.X., Dickerson, R.R., Chen, F., 2011a. Impact of upstream urbanization on the urban heat island effects along the Washington-Baltimore corridor. Journal of Applied Meteorology and Climatology 50, 2012–2029. https://doi.org/10.1175/JAMC-D-10-05008.1.

Zhang, K., Oswald, E.M., Brown, D.G., Brines, S.J., Gronlund, C.J., White-

Newsome, J.L., Rood, R.B., O'Neill, M.S., 2011b. Geostatistical exploration of spatial variation of summertime temperatures in the Detroit metropolitan region. Environmental Research 111, 1046 – 1053. http://www.sciencedirect.com/science/article/pii/S0013935111002118.

Zhao, L., Lee, X., Smith, R.B., Oleson, K., 2014. Strong contributions of local background climate to urban heat islands. Nature 511, 216–219. https://doi.org/10.1038/nature13462.

Zhou, J., Chen, Y., Zhang, X., Zhan, W., 2013. Modelling the diurnal variations of urban heat islands with multi-source satellite data. International Journal of Remote Sensing 34, 7568–7588. https://doi.org/10.1080/01431161.2013.821576.

Zhu, W., Lű, A., Jia, S., Yan, J., Mahmood, R., 2017. Retrievals of all-weather daytime air temperature from MODIS products. Remote Sensing of Environment 189, 152 – 163. http://www.sciencedirect.com/science/article/pii/S0034425716304503.

List of Figures